MULTI-SCALE INVERSION OF SUBSURFACE DATA AIMED AT CHARACTERIZING HETEROGENEOUS CARBONATE RESERVOIRS

ALIREZA SHAHIN[1], MIKE MYERS[2], PAUL STOFFA[3] and LORI HATHON[2]

[1] *Department of Geology, University of Isfahan, Isfahan, Iran. arshah2013@gmail.com*
[2] *University of Houston, Cullen College of Engineering, Houston, TX 77204, U.S.A.*
[3] *University of Texas at Austin, Institute for Geophysics, Austin, TX 78758, U.S.A.*

(Received November 26, 2020; revised version accepted March 17, 2021)

ABSTRACT

Shahin, A., Myers, M.T., Stoffa, P.L. and Hathon, L.A., 2021. Multi-scale inversion of subsurface data aimed at characterizing heterogeneous carbonate reservoirs. *Journal of Seismic Exploration*, 30: 319-345.

Inverting single-scale subsurface data have been adequately addressed in literature. Nevertheless, multi-scale inversion have not been broadly studied to fully characterize heterogeneous carbonate reservoirs. To address multi-scale inversion for carbonates, our research deals with core plugs, well logs and seismic data in the following three sequential stages:

• On the core scale, we make three independent porosity measurements (Archimedes, μCT, and NMR). Measuring electrical resistivity, P- & S-wave velocities on brine saturated core plugs along with joint modeling of the same properties using staged differential effective medium (SDEM) theory, help us to fine tune the model parameters through a global optimization algorithm. Core-calibrated multi-physics rock model provides micro- & macro-porosities which are consistent with NMR and μCT derived porosities.

• Next, we extend the technique from core to well log scale and demonstrate it using constructed logs from a real carbonate formation. In this stage, we integrate mass balance equations to model bulk density and SDEM theory to model elastic and electrical resistivity of dual-porosity carbonates. We design a stochastic global algorithm to simultaneously invert petrophysical properties. By constructing a dual-porosity formation, we demonstrate that the proposed workflow recovers the petrophysical properties.

0963-0651/21/$5.00

• Finally in the third stage, we propose an inversion algorithm in seismic scale to simultaneously retrieve P&S-wave velocities and density. Similar to core- & log-scale stages, Very fast simulated annealing (VFSA) is the special global optimization algorithm employed to minimize objective function. The optimization algorithm is stochastic in nature and is enable to estimate uncertainty in model parameters. Unlike commercial software, no assumption is made on correlations between P&S-wave velocities and density. No smoothed background model is needed and only bounds on model parameters are necessary.

KEY WORDS: multi-scale, inversion, carbonate, stochastic, optimization.

INTRODUCTION

It has been a while since the statistical rock physics (Mukerji et al., 2001a) has been introduced to the geosciences community to address inherent uncertainties involved in simplified physical relationships between petro-elastic attributes. Statistical rock physics combined with cross-plotting techniques have been performed to map probabilistic litho-fluid facies (Avseth et al., 2001; Mukerji et al., 2001b).

The most popular cross-plotting technique is called the rock physics template (RPT). In RPT analysis, the depositional and diagenetic trend models are combined with Gassmann fluid substitution to make cross-plots of elastic parameters, e.g., Poisson ratio versus acoustic impedance. Using the RPTs, one is able to distinguish the litho-fluid effects and to extract some of the petrophysical properties from inverted elastic parameters (Avseth et al., 2005). However, the RPTs are not universal and they need to be created for each individual petroleum basin. Besides, RPTs like other cross-plotting approaches lead to semi-quantitative and indirect estimates of petrophysical properties. Consequently, a direct inversion of seismic reflectivity data to petrophysical properties without intermediate graphical mapping of petro-elastic attributes is worthwhile to implement. This technique has been addressed by several authors. Multivariate statistical methods and neural networks (e.g., Fournier, 1989; Hampson et al., 2001) are designed to estimate petrophysical properties from seismic data. In these approaches linear and nonlinear relationships between seismic attributes, e.g., seismic amplitude, acoustic and shear impedances, etc., and petrophysical properties, e.g., porosity, are developed and calibrated at well locations and will be used to predict petrophysical properties far away from wells where only seismic observations are available. These methods do not rely on any forward modeling schemes, e.g., rock-fluid physics and seismic modeling. Also knowledge of the seismic wavelet is not required. However; the methodology is only successful in developed fields where borehole data are available for calibration and the entire expected ranges of desired petrophysical properties are spanned by several well locations (Hampson et al., 2001). As a result, methods based on rock-fluid physics and elasticity theories have been extensively used in recent years to predict petrophysical

properties from seismic data. Their physical foundations provide more predictive power than statistical and neural network methods because these methods are capable of identifying unknown lithology and fluid scenarios not encountered at the well locations.

In this research paper, we first invert core scale measurements. Next, we construct resistivity, elastic, and density borehole-derived well logs for complex carbonates and convert well logs into petrophysical properties using a novel inversion workflow. For doing so and similar to Shahin et al., (2020), we utilize Very Fast Simulated Annealing (VFSA), a global optimization machine. Grain density, grain bulk & shear moduli, salinity, critical porosity, electrical resistivity lithology exponents, elastic length scales, primary & secondary porosities, water saturation, are grain, fluid, fitting parameters, and petrophysical properties recovered. Finally, we extend our multi-scale inversion to seismic data and propose a salient workflow to jointly invert pre-stack seismic gathers into P&S-wave velocities and density.

PORE COMBINATION MODELING TO SIMULATE ELECTIRCAL RESISITIVITY

Electrical-resistivity (inverse of conductivity) has been widely utilized to evaluate the hydrocarbon content of petroleum reservoirs. At the heart of formation evaluation, there exists “Archie’s equation” (Archie, 1962) to compute water saturation knowing reservoir porosity, brine resistivity, lithology or cementation exponent (m), and saturation exponent (n).

While Archie’s model is mainly valid for single pore and clay free formations, other models have been proposed for complex rocks with multiple pore structure. Pore combination modeling (PCM) methodology (Myers, 1989, 1991) is one those models which expresses the contribution of each pore structure and its fluid content in permeability and resistivity. In fact, PCM is an extension of Archie’s model representing rocks with multiple pore structures. Thanks to a universal carbonate core measurements, Myers (1991) obtained Archie’s lithology exponents for vuggy, intergranular, and microporosity pore types of carbonate formations worldwide. As summarized by Shahin et al. (2020), the following equation gives the formation factor of a water-bearing rock with two pore structures:

$$F = \left(\frac{1}{\boldsymbol{\phi_i}}\right)^{\lambda_i} \left(\frac{\boldsymbol{\phi_i}}{\boldsymbol{\phi_{i+}\phi_v}}\right)^{\lambda_v} . \quad (1)$$

F is the ratio of the resistivity of 100% water-saturated rock to brine resistivity called formation factor. ϕ_i and ϕ_v are the fractional primary

(intergranular or micro) and secondary (vugs and cracks) porosities, respectively. $\phi_t = \phi_i + \phi_v$, is the total porosity. λ_i is the lithology exponent for primary pores, and λ_v is the lithology exponent for secondary pores. In the following, we will present new methodologies to obtain the primary and secondary lithology exponents using resistivity core measurements and well logs via global optimization. Fig. 1 represents the PCM methodology for a dual pore carbonate formation.

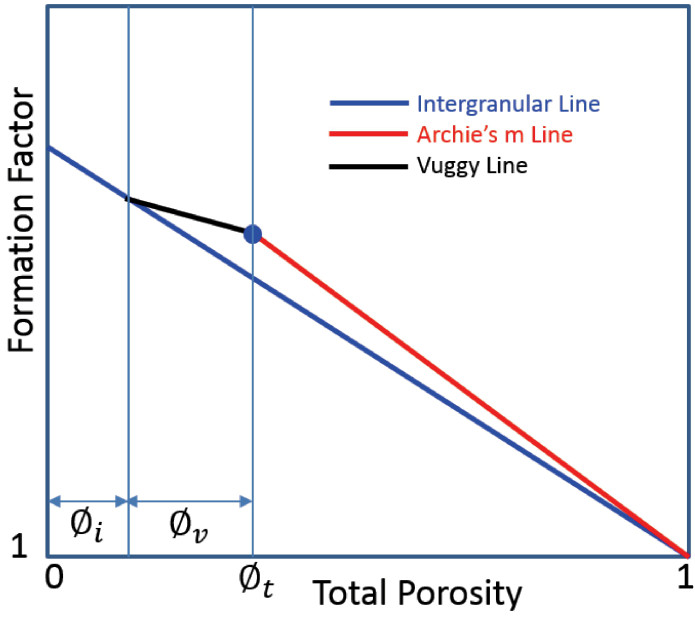

Fig. 1. A graphical representation of pore combination modeling (PCM). With the same notation by Shahin et al. (2020), the formation factor (F) and total porosity, i.e., F-ϕ_t are plotted in log-log plane. Starting from point (F=1 and ϕ_t=1) a blue line with slope of λ_i illustrates the gradual decrease in total porosity due to sediment compaction. At this stage, primary pores are the only pore system and total porosity (ϕ_t) is equal to primary porosity of ϕ_i. Then, diagenesis comes into play and secondary pores start to evolve. A black line with slope of λ_v represents the evolving of the secondary porosity of ϕ_v. This line has a different slope than the line of primary pores. When the diagenesis process is finished, the sample has a total porosity of ϕ_t which is the summation of ϕ_v and ϕ_t. The red line connecting the final position of sample in F-ϕ_t plane with the point of (F=1, ϕ_t=1) is the Archie's line with slope of (m) representing the lithology exponent (Shahin et al., 2020).

STAGED DIFFERENTIAL EFFECTIVE MEDIUM TO MODEL ELASTIC MODULI

Reuss lower bound and Voight upper bound have been historically utilized to associate the elastic moduli of rock components with the elastic moduli of the mixture. While the moduli of the mixtures are always located between these bounds (Mavko et al., 2020), several researchers attempted to better locate moduli exact position by adding more textural information on how grains and pores are structured within the rocks. One of such attempts was the work by Myers and Hathon (2012) who extended the differential effective medium theory by introducing the concept of "Staging" on how the process of sedimentation, lithification/ compaction, and diagenesis lead to form sedimentary rocks. In staged differential effective medium (SDEM) technique, inclusions of different length scale (aspect ratio) are gradually added to a host assuming they only feel the average properties of the host and neglecting interaction terms between the inclusions.

Similar to PCM to model resistivity, SDEM methodology models the elastic moduli of dual-porosity carbonates. In fact, PCM is a special case of SDEM, and these are general techniques for modeling the impact of mineralogy and texture on permeability, resistivity, and elastic measurements.

The well-known critical porosity (Nur et al., 1995) model is inherently included in SDEM (Myers and Hathon, 2012). To simulate the elastic moduli of a single-pore carbonate, we need a two-staged SDEM. The first step is to integrate the elastic moduli from host to the critical porosity with a length scale of L = 0 which mimics an iso-stress Reuss bound. The second step is to integrate from critical porosity to total porosity with a length scale of L#0 using:

$$M = M_c \frac{1+\left(\frac{\emptyset_c-\emptyset}{\emptyset_c}\right).\left(\frac{M_i-M_c}{M_c}\right).L}{1-\left(\frac{\emptyset_c-\emptyset}{\emptyset_c}\right).\left(\frac{M_i-M_c}{M_i}\right).(1-L)} \quad , \tag{2}$$

where, $\emptyset_c$ is the critical porosity, M_i is the inclusions' modulus, L is the length scale and related to this inclusion, and M_c is the iso-stress bound of the host and grain modulus at the critical porosity (Shahin et al., 2016).

A dual porosity carbonate can be simulated by adding an additional integration step to model the secondary porosity (Myers and Hathon, 2012). Fig. 2 illustrates the SDEM technique for a dual-porosity formation. The elastic moduli (bulk and shear) are plotted versus total porosity (ϕ_t). The bound corresponding to length scale of L_i connects the elastic moduli at critical porosity (M_c) to elastic moduli at zero porosity (Solid or grain

moduli). This bound is associated with primary pores. The bound corresponding to length scale of L_v which does not pass through elastic moduli at critical porosity is associated with the moduli change due to change in secondary porosity. For a formation consisting of primary and secondary pores the secondary-porosity bound intersects the primary bound at the primary porosity.

In the following, we will present new methodologies to obtain grain elastic moduli, critical porosity, primary and secondary's L parameters, and lithology exponents of each pore system from sonic and resistivity core measurements and well logs via global optimization.

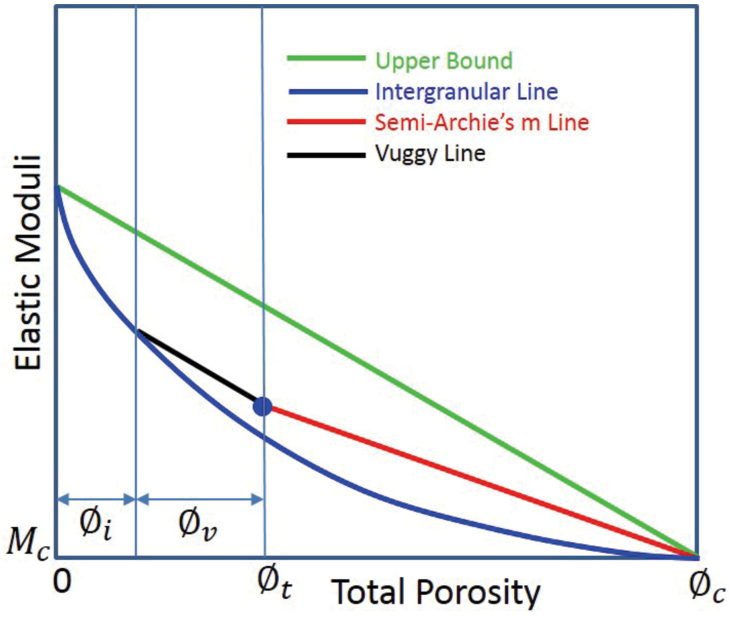

Fig. 2. Illustration of staged differential effective medium (SDEM) technique for a dual porosity carbonate. The elastic moduli of the mixture (M) and total porosity, i.e., M-ϕ_t are plotted in linear plane. ϕ_i is the primary porosity, ϕ_v is the secondary porosity, and the sum $\phi_t = \phi_{i+}\phi_v$, is the total porosity. Starting from point (ϕ_C, M_c) the blue bound with length scale of L_i illustrates the gradual decrease in total porosity due to sediment compaction. At this stage, primary pores are the only pore system and total porosity (ϕ_t) is equal to primary porosity of ϕ_i. Then, diagenesis comes into play and vugs start to evolve. A black bound with length scale of L_v represents the evolving of the secondary porosity of ϕ_v. This bound has a different length scale than the bound of primary pores. When the diagenesis process is finished, the sample has a total porosity of ϕ_t which is the summation of ϕ_v and ϕ_t. The red bound connecting the final position of sample in M-ϕ_t plane with the point of (ϕ_C, M_c) is the Semi-Archie's line described in Fig. 1.

MASS CONSERVATION TO REPLICATE BULK DENSITY

The following mass balance equations are used to replicate bulk density for core and well log measurements. For this particular exercise, we use tabulated calcite density of 2.71 g/cm^3, brine with density of 1.05 g/cm^3, and oil with density of 0.75 g/cm^3. In eqs. (3) and (4), ρ_b, ρ_{ma} , ρ_f, ρ_o, and ρ_w are bulk density, grain density, fluid density, oil density, and brine density, respectively. $\emptyset_t$ is the total porosity of $\phi_t = \phi_{i+}\phi_v$, and S_{wt} is the total water saturation occupying primary and secondary pores.

$$\rho_b = \rho_{ma}(1 - \emptyset_t) + \rho_f \emptyset_t \quad , \tag{3}$$

$$\rho_f = \rho_o(1 - S_{wt}) + \rho_w S_{wt} \quad , \tag{4}$$

MULTI-PHYSICS INVERSION OF CARBONATES IN CORE SCALE

Three independent porosity measurements on carbonate core plugs have been made. These include porosities obtained from Archimedes, micro-computerized tomography (μCT), and nuclear magnetic resonance (NMR). In Archimedes technique the weight of core plugs in dry, saturated and submerged conditions, pore volumes and porosity are determined. This technique is still the most accurate method to estimate total porosity. The porosity of core plugs using this method vary between 5 and 16 porosity units.

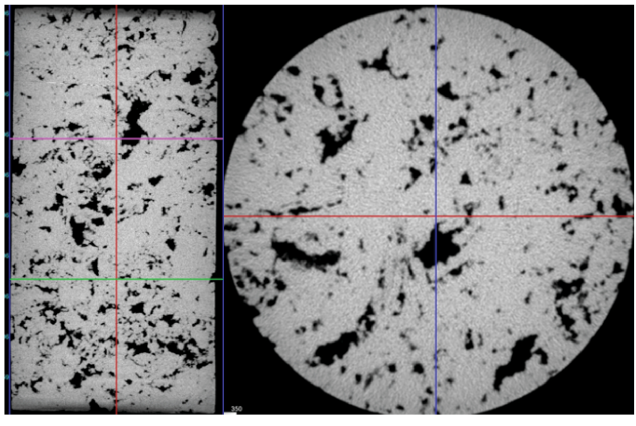

Fig. 3. Micro-CT scan of the carbonate core plug. The left image is a horizontal and the right one is a vertical slice through the 3D image acquired. Note that the majority of the pore volume are vugs and microporosity is not visible.

In μCT technique, X-rays are utilized to provide high-resolution images of geometry and microstructures. In Fig. 3, (Myers and Hathon, 2012) vertical and horizontal slices of the 3D volume are displayed. A significant portion of the pore type are vugs and no other visible pore type can be seen using μCT. We performed a segmentation technique using color classification to measure the vuggy porosity of the core plugs. On average, μCT-derived porosities are smaller than those estimated from Archimedes and NMR. This is consistent with the fact that μCT cannot resolve the microporosity.

NMR measures the porosity by application of a constant magnetic field followed by oscillating frequencies to measure the amount of protons processing around the constant magnetic field. The NMR measurements for porosity closely follow Archimedes porosities within 1 to 2 porosity unit. The smaller value for the NMR may be due to extremely small pores beyond the resolution of the NMR. Fig. 4 shows the T_2 distributions of samples used in this research. To better predict the contribution of each pore type, we choose to fit a Weibull distribution to NMR response. To estimate the model parameters for curve-fitting exercise a stochastic global optimization (Ingber, 1989, 1993) technique called very fast simulated annealing (VFSA) has been utilized. The detail of VFSA is summarized in the Appendix.

We choose to utilize the Weibull distribution as a base function for curve fitting. This is due to the fact that Weibull is a versatile distribution that can take on the characteristics of other types of distributions by varying the value of the shape parameter. One particular type of distribution which can be modeled via Weibull is Log-normal distribution. Log-normal distribution is of significant interest because grain size distribution is naturally a Log-normal distribution.

The probability density function (PDF) for Weibull distribution is given as:

$$f(x;\lambda,k) = \frac{k}{\lambda}\left(\frac{x}{\lambda}\right)^{k-1} \exp\left[-\left(\frac{x}{\lambda}\right)^{k}\right]$$

$$x \geq 0 \qquad k > 0 \ \ shape\ factor \qquad \lambda > 0 \ \ scale\ factor \quad . \qquad (5)$$

Most of the NMR T_2 distributions of our samples display bimodal behavior, so we add up two Weibull distributions with different weighting factors α_i as:

$$f(x;\lambda_1,k_1,\lambda_2,k_2,\alpha_1,\alpha_2) = \alpha_1 f_1(x;\lambda_1,k_1) +$$

$$\alpha_2 f_2(x;\lambda_2,k_2) \quad where \quad \alpha_1+\alpha_2 = 1 \quad . \tag{6}$$

The normalized error or objective function for the VFSA optimization is as follows:

$$\mathrm{E}(x;\lambda_1,k_1,\lambda_2,k_2,\alpha_1,\alpha_2) = \frac{2\sum_{i=1}^{n}[f(x_i)-NMR\ T2(i)]}{\sum_{i=1}^{n}[f(x_i)+NMR\ T2(i)]} \quad . \tag{7}$$

NMR T_2 data are discretized in T_2 domain with n the number of total samples and x is:

$$x = \ln\frac{T_2}{T_{2,0}} \quad . \tag{8}$$

$T_{2,0}$ is the smallest T_2 used in the T_2 distribution (here 0.01 ms). There are five independent model parameters, i.e., $\lambda_1, k_1, \lambda_2, k_2, \alpha_1$, to fit for each core plug. It worth noting that the extension of this approach to tri-modal distribution is straightforward where there will be 8 model parameters to fit the NMT T_2 distribution. The fitting can be formulated as a constrained non-linear optimization which we addressed via VFSA in this paper. The optimized model parameters have been used in decomposing the NMR T_2 response of all core plugs and then vuggy and microporosity of each core plug computed. Fig. 4 illustrates the NMR T_2 distribution and the associated bimodal Weibull distribution fits for one of the core plugs.

Analyzing the NMR response of all core plugs, we concluded that on average vugs contribute 80-95 percent of NMR total porosity and only a small fraction associated with microporosity. The NMR measurements provide convincing evidence that a dual pore system exists in these core plugs consisting of a connected microporosity with vugs. This information is vital for the SDEM resistivity and velocity modeling in the next part.

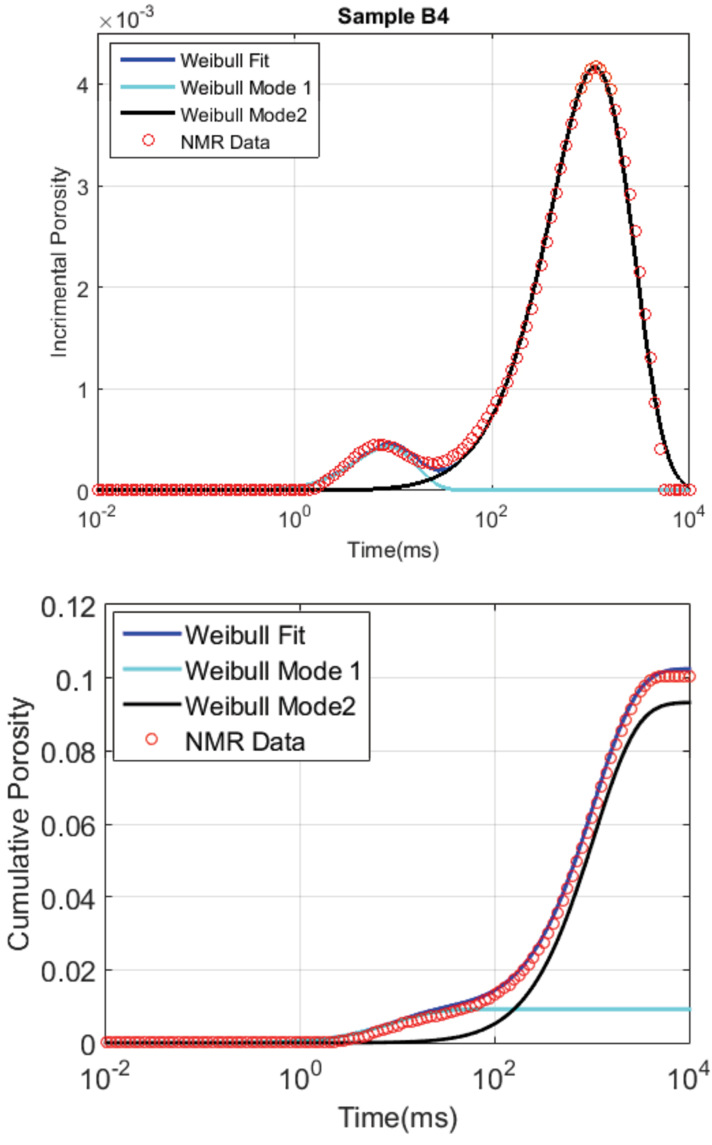

Fig. 4. Top panel shows NMR T_2 distribution and the associated bimodal Weibull distribution fit. The dots are NMR measurements (10 porosity unit). The solid black line is Weibull fit to the second mode or pore type which are vugs (9 porosity unit). The cyan solid line is the Weibull distribution of the first mode or pore type which is microporosity (less than 1 porosity unit). The bottom panel shows the cumulative distribution of NMR T_2 signal displayed in top panel.

The formation factor versus total Archimedes porosity is plotted in Fig. 5. The different blue lines all extrapolated to $\boldsymbol{F}$=1 and $\boldsymbol{\phi_t}$=1 are for $\boldsymbol{\lambda_m}$ from zero to three. One of these lines (red one) is the microporosity line best explained the petrophysical characteristics of these core plugs. There is a large scatter of these data about any of the lines because there are two pore types present and the amounts of both are changing. Fig. 6 displays the same data plotted in $\boldsymbol{F}$-$\boldsymbol{\phi}$ log-log plane. The microporosity trend line selected for the data set is obtained from the non-linear optimization. The position that vuggy porosity lines intersect the microporosity line will provide the amount of each individual porosity. The vuggy porosity computed from resistivity modeling along with the vuggy porosity derived from velocity modeling will be used later in an inversion machine to optimize model parameters of both velocity and resistivity models.

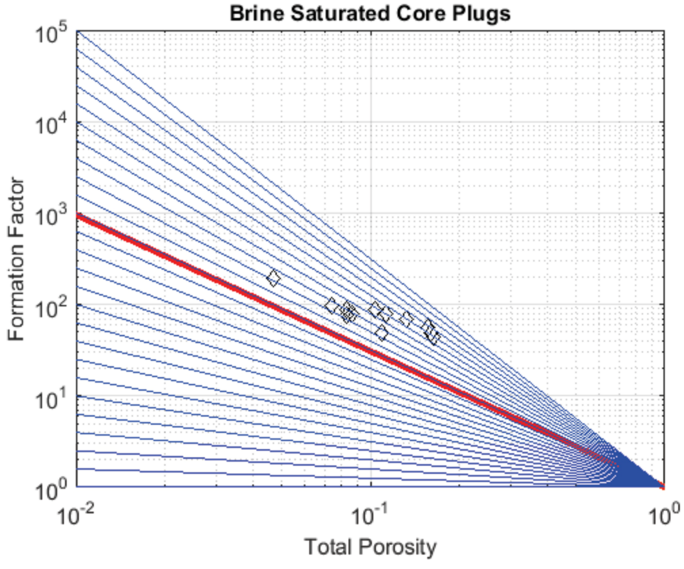

Fig. 5. Plot of the formation factor versus Archimedes porosity. No trend exists because there is a dual pore system of micro-pores and vugs.

Fig. 7 illustrates the Reuss and Voight average bounds for the carbonate core plugs. Different values of L for both bulk and shear moduli are also depicted. One of these lines (black one) is the microporosity line best explained the moduli of these core plugs. Similar to the resistivity model there is no obvious trend in these data because there are two pore types present and the amounts of both are changing. Fig. 8 displays the same data as shown in Fig. 7. The microporosity and vuggy porosity trends selected for the data set are obtained from the non-linear optimization of velocity and resistivity data. The position that vuggy porosity lines intersect

the microporosity line provides the amount of each individual porosity. The vuggy porosity computed from velocity modeling along with the vuggy porosity derived from resistivity modeling will be used later in an inversion machine to optimize the model parameters of both velocity and resistivity models.

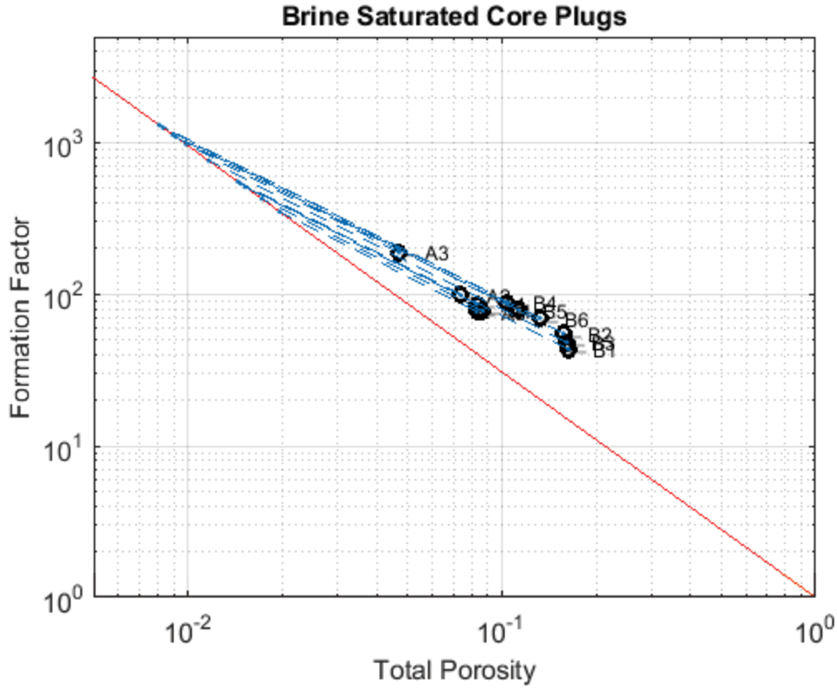

Fig. 6. Plot of the formation factor versus Archimedes porosity. The optimum microporosity lithology exponent (red line) is obtained from non-linear optimization. The dashed blue lines are optimum lithology exponent for vugs.

To optimize the SDEM model parameters, we define an objective function as the difference between vuggy porosities predicted from resistivity modeling ($\boldsymbol{\phi_i^{vr}}$) and the vuggy porosities computed from velocity modeling ($\boldsymbol{\phi_i^{vk}}, \boldsymbol{\phi_i^{vs}}$ for bulk and shear moduli, respectively) to be minimized. Index i indicates core plug numbers from 1 to n. During the optimizations process several constrained are applied. For instance, the computed moduli have to be always between Reuss and Voight average bounds. Microporosity curve in velocity modelling has to intersect vuggy porosity line for all the core plugs. Microporosity line in resistivity modeling has to intersect vuggy porosity line for all the core plugs.

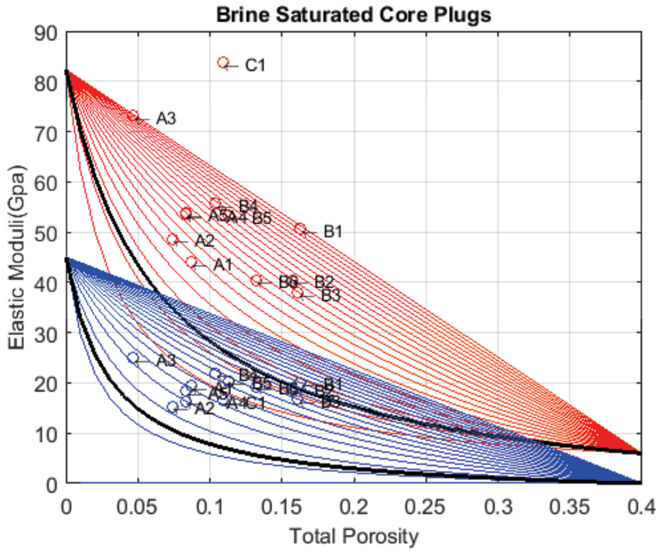

Fig. 7. Bulk and shear moduli versus Archimedes porosity. The red curves (bulk moduli) and blue curves (shear moduli) are for L = 0 to L = 1 spanning all the data unless C1 sample which is associated with an erroneous reading in P-wave traveltime. No trend exists because there is a dual pore system of micro-pores and vugs. The black curves are the optimum microporosity fits to the data.

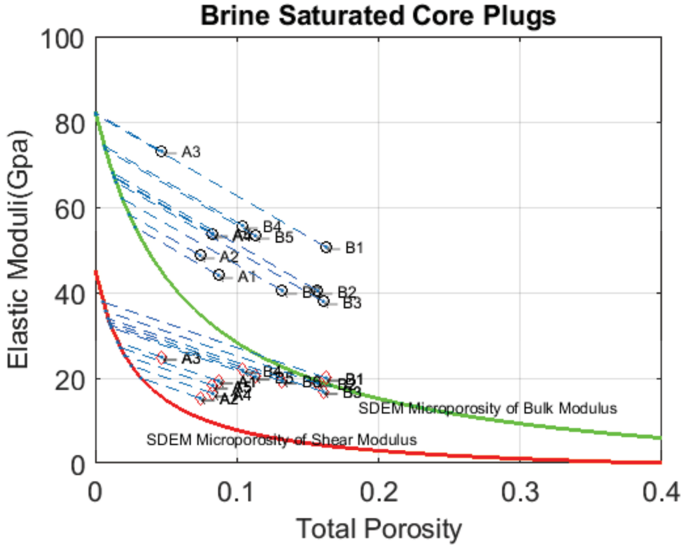

Fig. 8. Bulk and shear moduli versus Archimedes porosity. The optimum microporosity L parameters (red for shear and green for bulk modulus) are obtained from non-linear optimization. The dashed blue lines are drawn using the L = 1 for vugs.

$$\mathrm{E}(\phi_c, M_k, M_s, \lambda_m, \lambda_v, L_{ms}, L_{mk}) = \frac{2\sum_{i=1}^{n}[\phi_i^{vk} - \phi_i^{vs}]}{\sum_{i=1}^{n}[\phi_i^{vk} + \phi_i^{vs}]} + \frac{2\sum_{i=1}^{n}[\phi_i^{vk} - \phi_i^{vr}]}{\sum_{i=1}^{n}[\phi_i^{vk} + \phi_i^{vr}]} \quad . \qquad (9)$$

SDEM model parameters are critical porosity ($\boldsymbol{\phi_c}$), bulk ($\boldsymbol{M_k}$) and shear ($\boldsymbol{M_s}$) moduli of grains, microporosity lithology exponent for resistivity ($\boldsymbol{\lambda_m}$), vuggy porosity lithology exponent for resistivity ($\boldsymbol{\lambda_v}$), microporosity parameter for shear modulus ($\boldsymbol{L_{ms}}$), microporosity parameter for bulk modulus ($\boldsymbol{L_{mk}}$). Vuggy porosity L parameters for bulk and shear moduli are set to 1.0 based on the previously published results (Myers and Hathon 2012). Table 1 summarizes all the model parameters as well as their mean values for 200 runs of VFSA each with 200 iterations. Fig. 9 displays the correlation of vuggy porosity estimated from velocity and resistivity. It also shows a high correlation between vuggy porosity jointly estimated from velocity-resistivity and the ones estimated from NMR and μCT measurements.

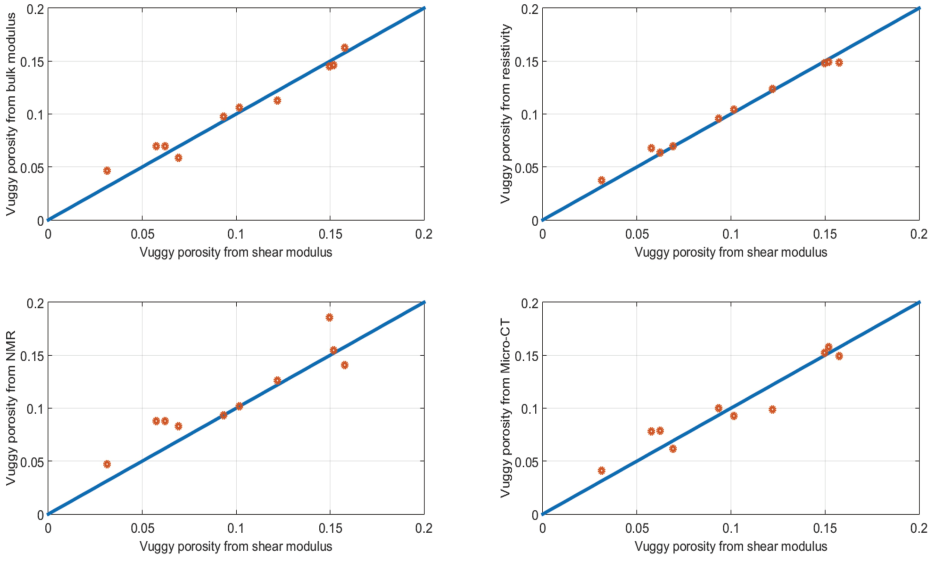

Fig. 9. Comparison of vuggy porosities estimated from different methods. The bottom panels (lower left and lower right) indicate high correlations between velocity-derived vuggy porosity (shear modulus here) and vuggy porosity from independent measurements of NMR and micro-CT.

Table 1. SDEM model parameters. Note that vuggy porosity L parameters for bulk and shear moduli are set to 1.0 based on the previously published results (Myers and Hathon 2012). The rest of parameters are obtained from VFSA optimization.

SDEM Model Parameters	Mean Value
Critical porosity	0.40
Bulk modulus (Gpa)	82.35
Shear modulus (Gpa)	45.08
L parameter for microporosity associated with bulk modulus	0.07
L parameter for microporosity associated with shear modulus	0.07
L parameter for vuggy porosity of bulk modulus	1.00
L parameter for vuggy porosity of shear modulus	1.00
Lithology exponent for microporosity associated with resistivity	1.49
Lithology exponent for vuggy porosity associated with resistivity	1.06

MULTI-PHYSICS INVERSION OF CARBONATES IN WELL LOG SCALE

As proven methodologies to simulate the effects of texture and lithology on elastic, resistivity, and permeability, PCM and SDEM are found satisfactory to model pore network of complex carbonates on core scale measurements. Now, we will extend this methodology to well log scale.

Fig. 10 displays a relatively thick carbonate reservoir with intergranular and vuggy porosities. The reservoir is divided to three separate zones including oil column on the top (~37 ft.), water leg in the bottom (~33ft.) and a transition zone (~10 ft.) in the middle portion of the carbonate formation. Note that we assume two different pore networks are fully connected and that is why intergranular water saturation and vuggy water saturation are equal to total water saturation. Table 2 summarizes the detail parameters of the carbonate reservoir.

Fig. 11 displays the simulated well log responses over the dual porosity carbonate formation shown in Fig. 10. Bulk density (ρ_b) is modeled using mass conservation equation, P-wave slowness (DTCO) & S-wave slowness (DTSM) modeled using SDEM, and electrical resistivity (R_t) using PCM. Model parameters are summarized in Table 2. As expected, distinct fluid zones are clearly separated on resistivity log in logarithmic scale and one can determine oil column, transition zone, and water leg from reservoir top to bottom, respectively. This trend can be seen on density and sonic logs in some degree, but it is not as clear as resistivity log due to the higher combination impact of porosity and saturation on sonic and density logs.

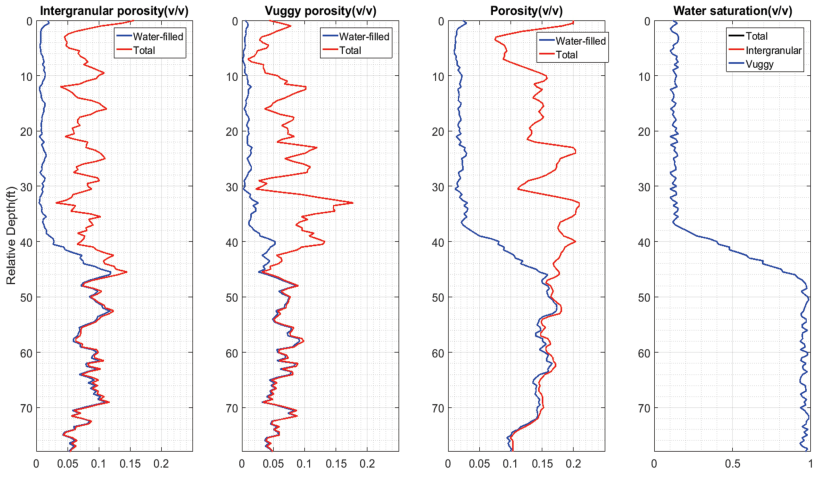

Fig. 10. Constructed petrophyscial properties of a carbonate reservoir. In the first three tracks from left, red curves are intergranular, vuggy, and total porosities, respectively. For the same tracks, blue curves are water-filled porosities. The first track from right shows intergranular water saturation, vuggy water saturation, and total water saturation which are equal at each depth interval.

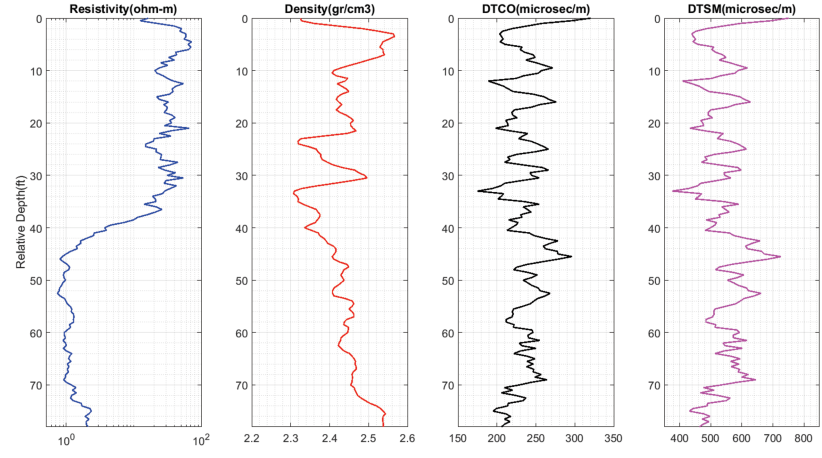

Fig. 11. Plots of the well log responses simulated with proposed multi-physics modeling over the dual porosity carbonate formation illustrated in Fig. 10. From left to right, the first track is electrical resistivity replicated with PCM, the second track is bulk density expressed by mass conservation, and the third and fourth tracks are compressional (P-wave) and shear (S-wave) slowness simulated with SDEM.

Table 2. Reservoir, grain, fluid, and model parameters for the dual porosity carbonate formation.

Properties	Symbol	Values	Units
Reservoir thickness	h	80	feet
Reservoir temperature	T	60	^{o}C
Irreducible water saturation	S_{wirr}	0.1	Fractional
Residual oil saturation	S_{or}	0.07	Fractional
Salinity	Sal	120	Kppm
Grain density	ρ_{ma}	2.71	gr/cm^3
Brine density	ρ_w	1.05	gr/cm^3
Oil density	ρ_o	0.75	gr/cm^3
Grain bulk modulus	K_{ma}	77	GPa
Grain shear modulus	μ_{ma}	32	GPa
Brine bulk modulus	K_w	2.5	GPa
Oil bulk modulus	K_o	0.75	GPa
Critical porosity	$\emptyset_c$	0.45	Fractional
Vuggy lithology exponent	λ_v	1.0	Fractional
Intergranular lithology exponent	λ_i	1.6	Fractional
Vuggy length scale for bulk modulus	L_v^k	1.0	Fractional
Intergranular length scale for bulk modulus	L_i^k	0.1	Fractional
Vuggy length scale for shear modulus	L_v^μ	1.0	Fractional
Intergranular length scale for shear modulus	L_i^μ	0.08	Fractional

We depict the RPT/MPRT in Fig. 12, where the cross-plots of resistivity and elastic properties (slowness, velocity, acoustic impedance, and velocity ratio) are displayed. The MPRT of this kind help interpreters to identify and separate litho-fluid facies. We intentionally utilize two different rock templates in this figure. The first one is traditional RPT (Avseth et al., 2005). These types of templates help seismic analysts to interpret seismic inversion results. For example, from the top left panel in this figure, one can conclude that oil-bearing and water-bearing zones can be separated using velocity ratio and acoustic impedance seismic attributes where all the points are color-coded by water saturation. From the top right panel in this figure, one can clearly see the gradual impact of intergranular porosity on velocity ratio and acoustic impedance seismic attributes where all the points are color-coded by intergranular porosity. The second kind of template is mainly derived from petrophysical properties including resistivity and compressional slowness (DTCO). These types of templates help petrophysicists to interpret well logs. For example, from the bottom left panel in this figure, one can conclude that oil-bearing and water-bearing zones can be separated using resistivity and DTCO well logs where all the points are color-coded by water saturation. From the bottom right panel in this figure, one can clearly see the gradual impact of intergranular porosity on resistivity and DTCO well logs where all the points are color-coded by intergranular porosity.

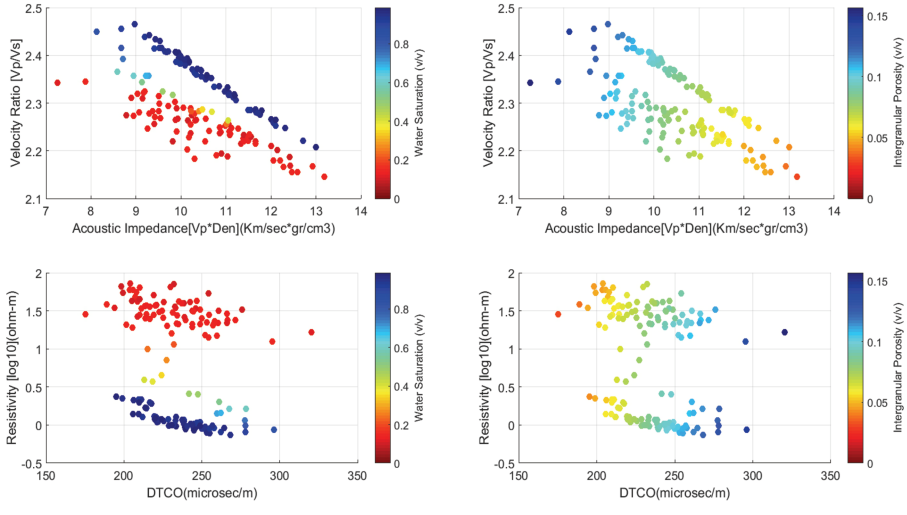

Fig. 12. Multiphysics rock templates created using different attributes. Left panels are color-coded with water saturation and highlight the separation of water-bearing from oil-bearing zones. Right panels are color-coded with intergranular porosity and highlight the impact of intergranular porosity on resistivity, velocity ratio, acoustic impedance, and P-wave slowness. See text for details.

As implemented by Shahin et al. (2020), we utilize the same optimization engine (VFSA) to minimize the objective function (See the Appendix for details). In this paper, an objective function is defined as the root mean square of differences between simulated and observed well logs including density, resistivity, and P&S-wave slowness logs (DTCO and DTSM). Two sets of parameters are defined in the optimization workflow.

Global parameters consist of grain density, grain bulk and shear moduli, salinity, critical porosity, intergranular lithology exponent for resistivity, intergranular L parameter (length scales) for bulk and shear moduli. Global parameters remain constant over the depth interval of interest. Vuggy's lithology exponent for resistivity as well as vuggy's L parameters for bulk and shear moduli are set to 1.0 based on the previously published results (Myers and Hathon, 2012). In VFSA optimization structure, we evaluate the global error function to update the global model parameters.

Local model parameters changing as functions of depth include intergranular porosity (φ_i), vuggy porosity (φ_v), total porosity (φ_t) and water saturation (S_w) at each depth interval. In VFSA structure, we evaluate the local error function to update the local model parameters in the corresponding depth interval.

We design an objective function which has three terms. The first term is the difference between resistivity well log data ($R^{obs.}$) and modeled resistivity ($R^{sim.}$) using the PCM methodology. The second and third terms are the difference between DTCO and DTSM well log measurements ($DTCO^{obs.}$ and $DTSM^{obs.}$) and their corresponding simulated logs using the SDEM model ($DTCO^{Sim.}$ and $DTSM^{Sim.}$). Note that all the terms are normalized to the summation of well log observations and simulated well log responses. This will facilitate the quality control of error (objective or cost) function.

$$\Delta E = \frac{\sum_{i=1}^{n}\left(R^{sim.} - R^{obs.}\right)^2}{\sum_{i=1}^{n}(R^{sim.} + R^{obs.})^2} + \frac{\sum_{i=1}^{n}\left(DTCO^{sim.} - DTCO^{obs.}\right)^2}{\sum_{i=1}^{n}(DTCO^{sim.} + DTCO^{obs.})^2}$$

$$+ \frac{\sum_{i=1}^{n}(DTSM^{sim.} - DTSM^{obs.})^2}{\sum_{i=1}^{n}\left(DTSM^{sim.} + DTSM^{obs.}\right)^2} \quad . \tag{10}$$

To converge the VFSA optimization and to obtain meaningful physical model parameters, we apply several constraints. Some of the important ones are as follows:

1. In each depth interval, the vuggy and intergranular porosities are smaller or equal to given total porosities.

$$\varphi_i \leq \varphi_t \tag{11}$$

$$\varphi_v \leq \varphi_t \tag{12}$$

2. In each depth interval, the sum of vuggy porosity and intergranular porosity should be equal to total porosities.

$$\varphi_i + \varphi_v = \varphi_t \tag{13}$$

3. The upper and lower search bounds on total porosity are computed from density log. Initial upper and lower bounds are first computed using a heavy mixture (heavy grain and water) and a light mixture (light grain and hydrocarbon), respectively. Then, safety factors in percentage are added to and subtracted from initial upper and lower bounds, respectively, to form conservative search bounds (Fig. 13).

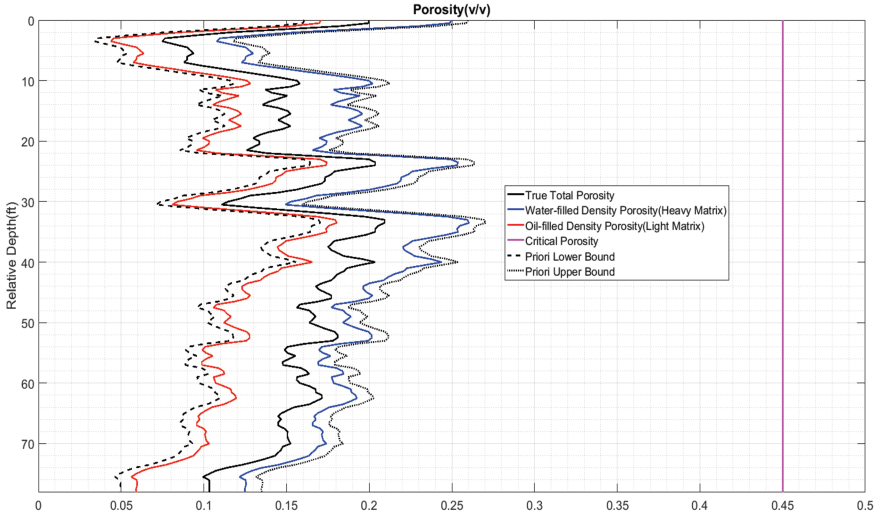

Fig. 13. Plot of true total porosity, true critical porosity, density porosities obtained from density log assuming know matrices and fluids, and lower and upper bounds on total porosity to be used in VFSA optimization.

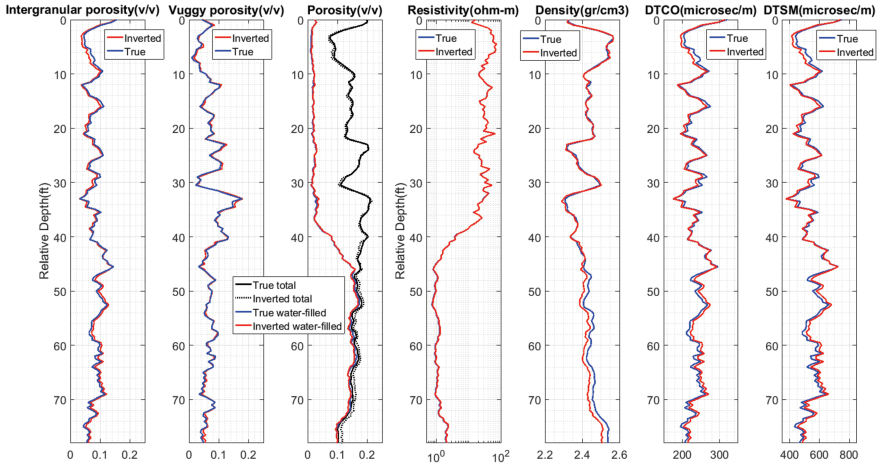

Fig. 14. Different tracks illustrating petrophyscial properties, associated well log responses, and their inverted values for one single realization. Dark blue curves display the true petrophysical properties and the associated well log responses, red curves show the inverted petrophysical properties and the inverted log responses. In the third track from left, true total porosity is shown in continuous black, the inverted total porosity in dotted black, true water-filled porosity in blue and inverted water-filled porosity in red.

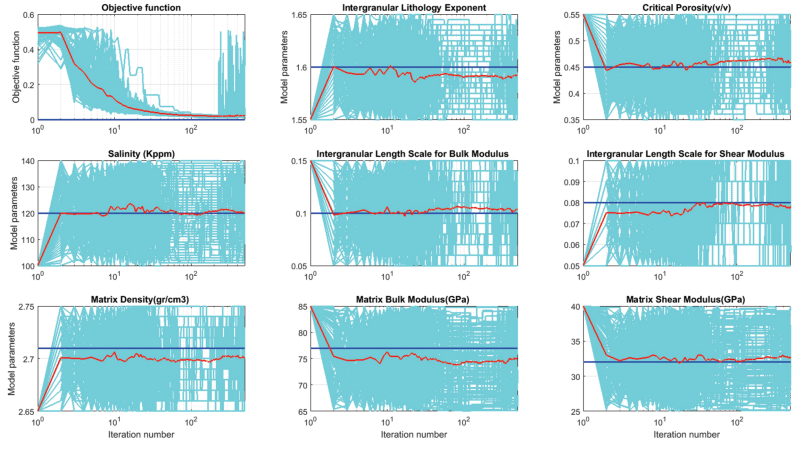

Fig. 15. Evolution of normalized objective (error or cost) function, grain and fluid properties, and PCM-SDEM model parameters. In all panels, blue curves are true or expected values, red curves are inverted parameters obtained from the averaging of 100 independent realizations shown in cyan color.

In Fig. 14, single realizations of true and inverted petrophysical properties and associated well log responses are overlaid in different panels. Note that petrophysical properties (intergranular, vuggy, total, and water-filled porosities) and well logs (Resistivity, DTCO, DTSM, and Density) are estimated precisely in oil column, water leg, and transition zone.

Fig.15 shows the performance of inversion workflow to recover global parameters by minimizing the normalized objective function. Note that the mean value of 100 realizations is close to the true value of each global parameter.

MULTI-PHYSICS INVERSION OF CARBONATES IN SEISMIC SCALE

Now, we utilize SDEM technique (already applied on core data and well logs) to replicate P&S-wave well logs. Then, we use full elastic reflectivity algorithm (Kennett, 1983) to simulate pre-stack seismic gathers. Finally, a novel stochastic seismic inversion method is designed to retrieve elastic properties and bulk density. Conditioned and NMO-corrected pre-stack seismic gathers in time and slowness domains are the main input. Inversion process can be executed in two different modes by replicating either NMO-corrected or raw synthetic gathers. In the latter mode, raw gathers are generated and NMO-correction is applied internally on raw gathers using intermediate P-wave velocity in each iteration. Full elastic reflectivity is the forward modelling algorithm utilized to replicate pre-stack seismic gathers. VFSA is the special global optimization algorithm employed to minimize objective function. The optimization algorithm is stochastic in nature and is enable to estimate uncertainty in model parameters. Unlike commercial software, no assumption is made on correlations between P&S-wave velocities and density. No smoothed background model is needed and only bounds on model parameters are necessary. The proposed workflow is claimed to recover sharp boundaries. This is due to the fact that non-liner full elastic reflectivity is used instead of linearized Zoeppritz equations. Thin beds are also recovered for the same reason and because of high resolution model parameters provided by stochastic component of the workflow.

We intend to use VFSA which naturally has a higher chance to find the global optimum of the objective function. In this paper, an objective function is defined as the root mean square of differences between simulated and observed pre-stack seismic gathers. The model parameters are locally time-dependent variables. These parameters are P-wave velocity, S-wave velocity, and density. During the optimizations process appropriate constraints are applied.

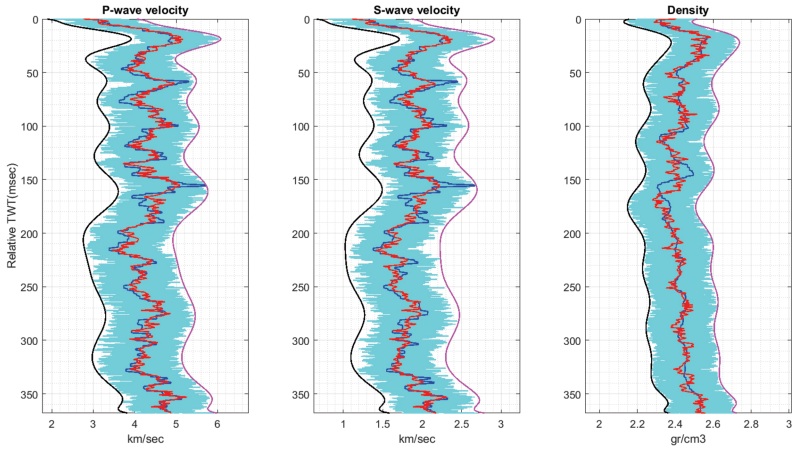

Fig. 16. Plots of the true well log responses and their inverted values over a thick dual-porosity carbonate formation containing intergranular and vuggy pores. In all tracks, blue curves are true well log responses, red curves are inverted properties obtained from the averaging of 50 independent realizations. Soft and stiff bounds are also displayed in black and pink, respectively.

Fig. 16 illustrates a relatively thick and dual-porosity carbonate which is partially saturated with oil for the upper part of the formation. The residual water saturation in the upper portion is about 10%. The lower portion is fully water saturated. The middle part is the transition zone. To model the density log, calcite with density of 2.71 g/cm^3, brine with density of 1.05 g/cm^3, and oil with density of 0.75 g/cm^3 are used. P&S-wave velocities are modelled using SDEM, matrix bulk and shear moduli of 77 and 32 GPa and a critical porosity of 0.45.

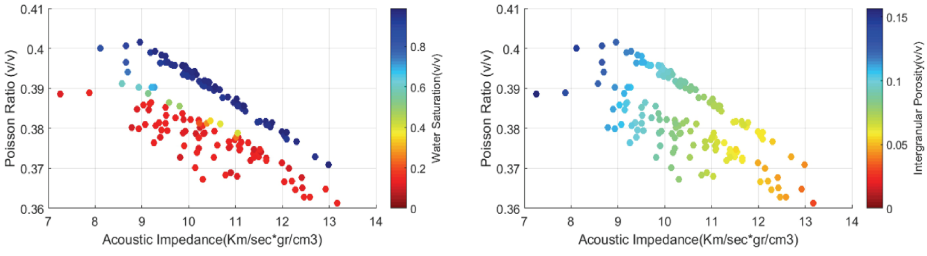

Fig. 17. Cross plots of the true well log responses for the dual-porosity carbonate formation containing intergranular and vuggy pores. Left panel is color-coded with water saturation and right panel with intergranular porosity.

As can be seen in Fig. 16, the inversion workflow is capable of matching the model for the three portions of carbonate formation (water leg, oil column, and transition zone) and retrieving P-wave velocity, S-wave velocity, and density with high precision. Note that the mean value of 50 realizations is very close to the true value of properties.

Fig. 17 shows the rock physics cross plots for dual-porosity carbonate formation displayed in Fig. 20. As seen, water leg and oil column can be separated using the left panel. Gradual decrease in acoustic impedance and increase in Poisson's ratio are the indication of increase in intergranular porosity (right panel).

Fig. 18 shows the performance of inversion workflow to match true and synthetic pre-stack seismic gathers. As seen, the difference between true and mean synthetic gathers are close to zero and this emphasizes the power of the inversion machine.

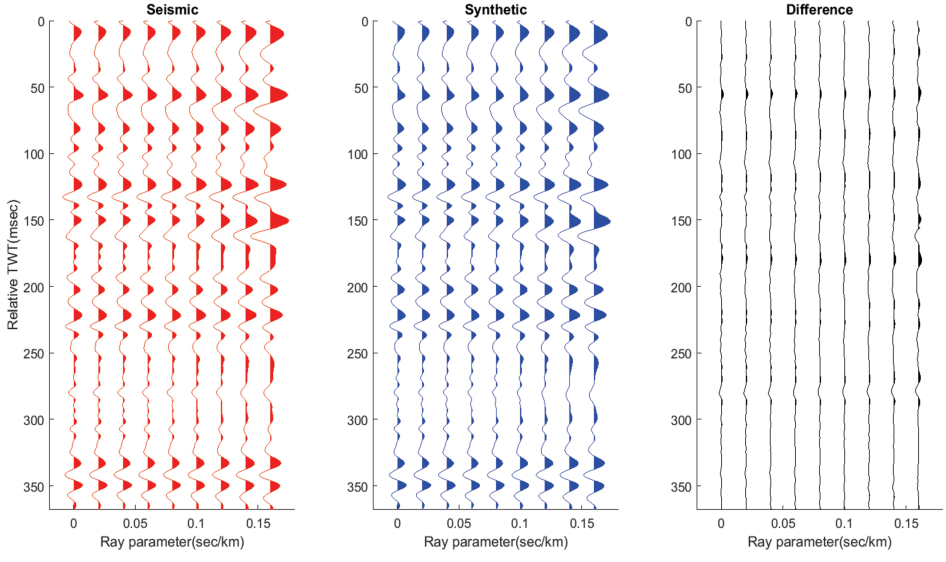

Fig. 18. Plots of the true (left track) and synthetic seismic (middle track) responses over the dual-porosity carbonate formation. Full elastic reflectivity is utilized as the modeling algorithm. The right track is the difference between true and synthetic seismic. Note that synthetic response is simulated for P&S-wave velocities and density obtained from the averaging of 50 independent realizations.

CONCLUSION

On core scale, we propose the PCM-SDEM technique to simultaneously simulate the resistivity and velocities data for complex carbonate formations. The proposed methodology consistency estimate micro-& vuggy porosities from the data of various physics. The technique also assists petrophysicists and geophysicists by providing petro-electro-elastic models which are verified by other complementary data such as nuclear magnetic resonance and micro-computerized tomography.

On well log scale, we propose an integrated multiphysics technique to simultaneously replicate resistivity, density, and the elastic responses of dual pore carbonates. We construct the well log responses using the multiphysics models. We then design a customized VFSA search engine to perform an innovative inversion algorithm. The significant parameters recovered through the optimization algorithm are grain properties (density and elastic moduli), salinity, critical porosity, resistivity-sonic model parameters, intergranular porosity, vuggy porosity, total porosity, and water saturation. In the proposed workflow, one can seamlessly quantify the uncertainty of global and local model parameters. For doing so, we randomly initialize the VFSA optimization several times and obtain independent realizations at each iteration.

Finally, we extend our multi-scale inversion to seismic data and propose a salient workflow to jointly invert pre-stack seismic gathers into P&S-wave velocities and density. Elastic and density well logs have been constructed using SDEM and mass balance equations for a relatively thick dual-porosity carbonate reservoir. Then, pre-stack seismic gathers are simulated using full elastic reflectivity seismic modelling. Then, a stochastic global optimization algorithm has been designed to invert pre-stack seismic gathers. Locally time-dependent P&S-wave velocities and density are the main properties estimated via this inversion algorithm. Uncertainty estimation of retrieved properties is a natural outcome of the proposed workflow. Uncertainty of these properties will be quantified via independent implementation of the stochastic optimization initialized with random model parameters.

Our future research will be to invert pre-stack seismic data directly into petrophysical properties. The products of such an inversion will be mineralogy, pore-type, porosity, and water saturation of carbonate reservoirs.

REFERENCES

Archie, G.E., 1962. The electrical resistivity log as an aid in determining some reservoir characteristics. Transact. AIME, 146: 54-67.

Avseth, P., Mukerji, T. and Mavko, G., 2005. Quantitative Seismic Interpretation. Cambridge University Press, Cambridge.

Avseth, P., Mukerji, T., Jorstad, A., Mavko, G. and Veggeland, T., 2001. Seismic reservoir mapping from 3-D AVO in a North Sea turbidite system. Geophysics, 66: 1157-1176.

Bruggeman, D.A.G., 1935. Berechnung verschiedener physikalischer Konstanten von heterogenen Substanzen. I. Dielektrizitätskonstanten und Leitfähigkeiten der Mischkörper aus Isotropen Substanzen. Annalen Physik, 416: 636-664.

Ellis, D. and Singer, J., 2007. Well Logging for Earth Scientists, 2nd Ed. Springer Verlag, New York.

Fournier, F., 1989. Extraction of quantitative geologic information from seismic data with multidimensional statistical analysis: Part I, methodology, and Part II, a case study. Expanded Abstr., 59th Ann. Internat. SEG Mtg., Dallas: 726-733.

Gassmann, F., 1951. Über die Elastizität an Porösen Medien. Vierteljahrsschrift der Naturforschenden Gesellschaft, 96: 1-23.

Hampson, D.P., Schuelke, J.S. and Quirein, J.A., 2001. Use of multiattribute transforms to predict log properties from seismic data. Geophysics, 66: 220-236.

Ingber, L., 1989. Very fast simulated re-annealing. Mathemat. Comput. Modell., 12: 967-973.

Ingber, L., 1993. Simulated annealing: Practice versus theory. Mathemat. Comput. Modell., 18: 29-57.

Kennett, B.L.N., 1983. Seismic Wave Propagation in Stratified Media. Cambridge University Press, Cambridge.

Mavko, G., Mukerji, T. and Dvorkin, J., 2020. The Rock Physics Handbook, 3rd Ed. Cambridge University Press, Cambridge.

Myers, M.T., 1989. Pore combination modeling: extending the Hanai-Bruggeman equation. SPWLA 30th Ann. Logging Symp., 1989-D.

Myers, M.T., 1991. Pore combination modeling: A technique for modeling the permeability and resistivity of complex pore systems. SPE Ann. Techn. Conf., 22662-MS.

Myers, M.T. and Hathon, L.A., 2012. Staged differential effective medium (SDEM) models for the acoustic velocity in carbonates. Am. Rock Mechan. Assoc., 12-553.

Mukerji, T., Jørstad, A., Avseth, P., Mavko, G. and Granli, J.R., 2001a. Mapping lithofacies and pore-fluid probabilities in a North Sea reservoir: Seismic inversions and statistical rock physics. Geophysics, 66: 988-1001.

Mukerji, T., Avseth, P., Mavko, G., Takahashi, I. and González, E.F., 2001b. Statistical rock physics: Combining rock physics, information theory, and geostatistics to reduce uncertainty in seismic reservoir characterization. The Leading Edge, 20: 313.

Nur, A., Mavko, G., Dvorkin, J. and Gal, D., 1995. Critical porosity: the key to relating physical properties to porosity in rocks. Expanded Abstr., 65th Ann. Internat. SEG Mtg., Houston: 878.

Raymer, L.L., Hunt, E.R. and Gardner, J.S., 1980. An improved sonic transit time to porosity transform. Expanded Abstr., 21st Ann. Logging Symp., Soc. Profess. Well Log Analys., P546.

Sen, M.K. and Stoffa, P.L., 2013. Global Optimization Methods in Geophysical Inversion, 2nd Ed. Cambridge University Press, Cambridge.

Shahin, A., Myers, M.T. and Hathon, L.A., 2020. Global optimization to retrieve borehole-derived petrophysical properties of carbonates. Geophysics, 85(3): D75-D82.

Shahin, A., Stoffa, P.L. and Myers, M.T., 2020. Stochastic seismic-wavelet inversion toward carbonate quantitative interpretation. Extended Abstr., 82nd EAGE Conf., Amsterdam.

APPENDIX

VERY FAST SIMULATED ANNEALING (VFSA) OPTIMIZATION

One needs to consider a global optimization algorithm when dealing with significant non-linearity in the cost/error function, otherwise optimizing the error function might lead to finding local minima/maxima in inversion process. Several authors find VFSA (Ingber, 1989, 1993), as an amazing optimizer which not only is a global search engine, but also a stochastic one. Monte Carlo Guided (MCG) search is at the heart of VFSA. Samples in model space are taken using MCG from 1D Cauchy distribution which is a function of so call temperature. Similar to solid heating process and gradual cooling until reaching to minimum energy state, VFSA has already have several applications in geosciences and petroleum engineering (Sen and Stoffa, 2013).